Three-dimensional carbon foam nanocomposites for thermal energy storage

Oluwafunmilola Ola, Yu Chen, Yanqiu Zhu*

College of Engineering and Physical Sciences, University of Exeter, EX4 4QF, UK

ARTICLE INFO

ABSTRACT

Nanocomposites consisting of paraffin/graphene nanoplatelets mix embedded in carbon foams via vacuum infiltration were fabricated with the aim of developing new phase change material (PCM) formulation with excellent shape stabilization, improved thermal conductivity and outstanding thermal reliability and structural stability. Physicochemical and thermal properties of the nanocomposites were evaluated using a suite of techniques such as scanning and transmission electron microscopy, X-ray diffraction, attenuated total reflection - Fourier transform infrared spectroscopy, nitrogen adsorption analyzer, differential scanning calorimetry, mechanical tester, Raman spectroscopy, thermal conductivity analyzer and thermogravimetric analyzer. The carbon foams exhibited good cyclic compressive behavior at a strain of up to 95% and kept part of their elastic properties after cyclic testing. Due to the robust mechanical integrity and layered meso-/macroporous morphology of these carbon foams, the nanocomposites are well equipped to cope with volume changes without leaking during thermal cycling. A 141% thermal conductivity enhancement observed for the carbon foam nanocomposite demonstrates the contributing role of the carbon foam in creating effective heat transfer through its conductive 3D network. The results have shown that proper chemical modification and subsequent carbonization of the low cost porous foams can lead to ultralight multifunctional materials with high mechanical and physical properties suitable for thermal energy storage applications.

1. Introduction

Technologies based on phase change materials (PCM) have shown great promises for space heating applications due to their large energy storage capacity, high heat of fusion and isothermality during charging and discharging cycles. In PCM systems, energy storage is achieved via phase change from gas–liquid, solid–solid or liquid–solid; and solid–liquid PCM systems are often preferred due to smaller volume variation with enthalpy during the sensible heat accumulation. The selection of appropriate PCMs is influenced primarily by the cost and operating temperature range of applications. Other key factors include specific heat capacity, thermal conductivity and latent heat per unit mass of the PCM. Several organic and inorganic PCMs such as paraffin wax, salt hydrates, metals and alloys have been extensively tested as energy storage materials. Compared with inorganic PCMs that have higher volumetric heat storage capacity, some organic PCMs are not limited by supercooling and incongruent melting during phase change [1]. Paraffin wax has been widely investigated for latent heat thermal energy storage (TES) due to its target oriented discharging behavior, low cost, small supercooling, low vapor pressure and high chemical and thermal stability at temperatures below 500 °C over several charging/discharging cycles [1]. However, they generally suffer from low thermal conductivity and poor structural integrity during the change from solid to liquid phase. Liquid leakage often restricts the applicability of paraffinic based PCM materials due to reduced energy storage capacity and difficulty in extraction during thermal cycling [2].

The concept of micro-structured composites with different chemically compatible components has been proposed to overcome these limitations. Dispersion of different carbon allotropes or other highly conductive materials such as multi-walled carbon nanotubes and metallic materials in organic PCMs has been attempted to enhance the thermal conductivity for low temperature applications [3–5]. Metallic fins have also been integrated into PCM systems to increase the thermal conductivity, however the cost and weight of such storage systems are increased significantly [2]. Other strategies including PCM encapsulations or the addition of a nucleating agent have also been investigated to suppress the supercooling. During the PCM encapsulation, heat transfer was increased while liquid leakage and interaction of the PCM with external environment were prevented [6]. Although some organic PCMs like paraffin wax are incompatible with plastic containers, they are compatible with most metallic containers [1]. Conversely, supporting materials like high density polyethylene, diatomite, styrene-

---

butadiene-styrene copolymer etc. have been used for shape stabilization during phase change through the polymer framework to prevent liquid leakage [7]. Clay materials such as montmorillonite have also been used to stabilize the PCM, due to their high sorption capacity which enhances the dispersion of the PCM [8].

Three-dimensional (3D) polymer materials have been applied for different commercial and industrial applications such as catalysis, insulation and acoustic absorption where combined properties of low weight, flexibility and absorption capacity are required [9,10]. Thermal, mechanical and electrical properties of these low-density materials have been reported to be linked to their interconnected cellular networks, shape, size and cell parameters [10]. Recently, compressible porous materials with interconnected structures have been utilized in environmental applications due to several unique features such as ease of regeneration and reuse [9]. Therefore, composites comprising 3D porous materials with conductive nanofiller is believed to be an effective strategy, because they will not only enhance the thermal conductivity but also decrease the overall weight. Meanwhile, their high absorption capacity and robust mechanical integrity will allow for these nanocomposites to address the liquid leakage problem associated with the volume change in paraffin wax-based PCM systems [6].

In this work, we present a scalable one-step method for the fabrication of 3D porous carbon nanocomposites that possess excellent mechanical properties that are highly beneficial to shape stabilization during thermal cycling. The novel porous carbon nanocomposite which consists of 3D carbon foam as the supporting material (SM), paraffin wax (53–57 °C, ASTM D 87) as the PCM, and graphene nanoplatelets (GNPs) mixture as the thermal enhancement material (TEM) were studied for TES applications and the optimum nanocomposite formulation was determined. We demonstrate that the resulting nanocomposites exhibit enhanced thermal conductivity, improved thermal stability and high reliability during cycling without increasing the overall weight, as measured by thermal conductivity analyzer, thermogravimetric analyzer and differential scanning calorimetry.

2. Experimental

2.1. Preparation of PCM mix and carbon foam nanocomposites

Carbon foams were fabricated by a one-step pyrolysis of a porous template (melamine-formaldehyde sodium bisulfite copolymer, $C_4H_8N_6O$, Avocation Ltd) in an inert atmosphere at several temperatures (i.e. 800, 900, 1000, 1100 and 1200 °C) followed by a chemical vapor deposition (CVD) treatment with acetonitrile (CH_3CN, 99.8%, Sigma Aldrich) as carbon and nitrogen source (injection rate: 0.08 ml/min) at 850 °C for 2 h. The CVD treatment was employed to improve the carbon content since the carbon yield of materials derived from melamine precursors has been reported to possess low carbon content of 9% [9]. The nomenclature adopted for the foams was according to their carbonization temperatures. For example, the CF obtained at 1000 °C is referred to as CN10. A PCM mix consisting of 2 wt% graphene nanoplatelets (Sigma Aldrich) mixed with liquid paraffin wax (mp. 53 – 57 °C, ASTM D 87, Sigma Aldrich) was used as the latent heat storage material. The PCM mix was subjected to a magnetic mixing (James, Sonic-6D) and ultrasonication (Camlab, MS-H280-Pro) treatment, prior to being introduced into the meso-/macroporous carbon foam matrix via a vacuum infiltration at 200 mbar using a Buchner funnel with a diameter of 25 cm attached to a rotary vane pump (Marvac Scientific, E-A-10). Mass fraction of PCM mix in the nanocomposite was ~ 96%. The composites were then trimmed with a blade to squares of 1 × 1 cm, with a thickness of 0.1 cm, for further testing.

2.2. Characterization

Morphological and elemental analyses of the carbon foam and its subsequent nanocomposites were carried out using scanning and transmission electron microscopy (Hitachi S3200N, Oxford instrument - SEM-EDS and JEOL-2100 - HR-TEM), operated at 20 and 200 kV, respectively. Three-dimensional (3D) images of the foams were recorded by microtomography (micro-CT) with an X-Tek Benchtop 160Xi CT machine. Crystalline phase of the nanocomposite samples was examined by X-ray diffraction (XRD, Bruker D8 diffractometer) measured with a Cu Kα radiation (40 kV, 40 mA), at a step size of 0.02° and dwell time of 1 s. Interaction between the PCM mix and carbon foams was evaluated using attenuated total reflection - Fourier transform infrared spectroscopy (ATR-FTIR) with an Alpha FTIR system with Platinum ATR setup (Bruker) over a wavelength range of 400–4000 cm^{-1}. The pore distribution of the foam was measured on a nitrogen adsorption analyzer. Thermal properties such as specific heat and thermal stability were measured on a Mettler Toledo DSC 821e/700 system with measurement uncertainty of $\pm$ 2%, at a temperature range of 20–80 °C, heating and cooling rate of 5 °C/min under N_2 flow. Raman spectra were recorded with a 6 mW laser power at a 532 nm laser excitation. Thermal diffusivities of the nanocomposites were measured using a NETZSCH LFA 467 HyperFlash machine with measurement uncertainty of $\pm$ 2%. Thermal conductivity was extrapolated from the dataset obtained from thermal diffusivities, using λ = αρCp, where ρ and Cp represent the density and specific heat capacity, separately. An average thermal conductivity value was obtained after 3 separate runs. The cyclic compression test of the carbon foams was carried out on a Lloyds EZ20 advanced universal mechanical testing system, using a 500 N detection cell at a loading rate of 8 mm/min. Thermogravimetric analysis (TGA) was carried out using a TA SDT Q600 instrument with measurement uncertainty of $\pm$ 2 °C, at a ramping rate of 5 °C min^{-1} under Ar atmosphere. Shape stabilization was evaluated by subjecting the samples to elevated temperatures within the range of 30–90 °C on a hot stage for 5 min, followed by recording their form stability via digital photography, because shape stability is critical during thermal cycling that cause dimensional changes. Thermal distribution was also evaluated using an infrared thermal imager (Fluke C2) after the carbon foam nanocomposites were subjected to a constant temperature of 80 °C at different time intervals (0–70 s). The porosity was obtained using Eq. (1), as a fraction of the void volume in the total volume where V_{void}, V_{total} and V_{solid} represents volume of pores, total or bulk volume of the foam including the solid and pore volume and volume of solid, respectively [9]. V_{total} is extrapolated from the volume of the foam i.e. cube foam (a × b × c) and V_{solid} is calculated M/ρ (M and p represents foam weight and density of material). Density is defined as mass divided by the volume.

$$\Theta = V_{void}/V_{total} \times 100\% = 1 - V_{solid}/V_{total} \times 100\% \tag{1}$$

3. Results and discussion

3.1. Structural and physicochemical properties

After carbonization and CVD treatment, all carbon foams possess an interconnected, open cell, and meso-/macroporous network structure linked with concave shaped fibers, with porosity of ~ 99% (volume weight) and density within the range of 5–6.5 mg/cm^3 using Eq. (1) (Figs. 1 a-c & 2a). The density value is lower than those reported by several groups that used similar polymeric templates [10,11]. Based on the EDS results, the carbon foams are composed mainly of carbon and nitrogen, with nitrogen decreasing with increased high carbonization temperatures from CN8-CN12. Spherical nanoparticles are observed attached onto the surface and walls of the carbon foam prepared at temperatures from 1000 °C, (Fig. 1b) with big clusters of interlinked spherical particles observed for CN12, Fig. 1c). Further SEM-EDS analyses have confirmed that these particles consist of carbon. The crystallinity of the foams changed from amorphous to graphitic from CN8-CN12, with diffraction spots confirming the higher structural order
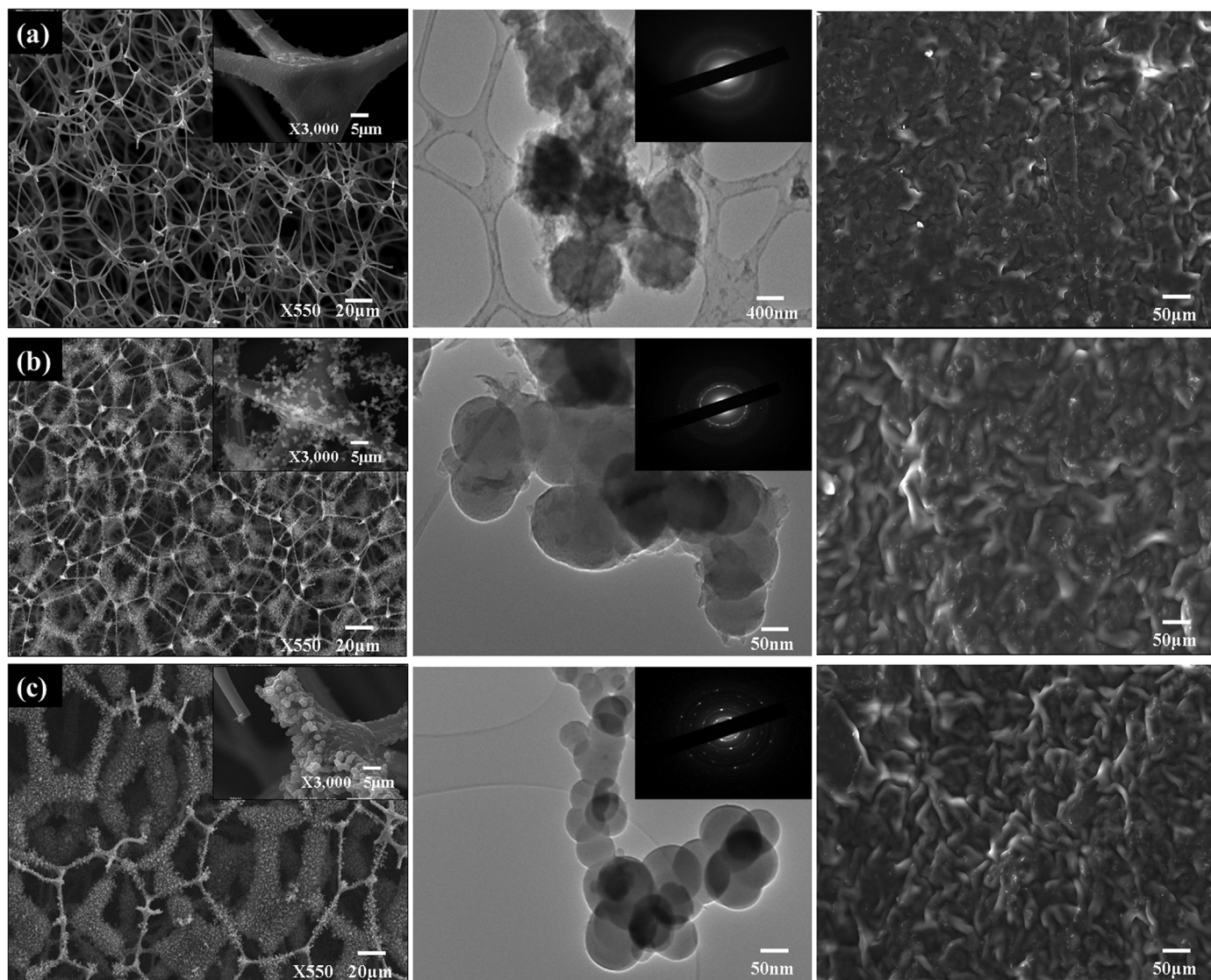
Fig. 1. SEM and TEM images of carbon foams and corresponding nanocomposites where a-c represents, CN8, CN10 and CN12, respectively (Left: SEM images showing foam morphology; middle: TEM and SAED pattern; right: SEM images of the foams after PCM infiltration).
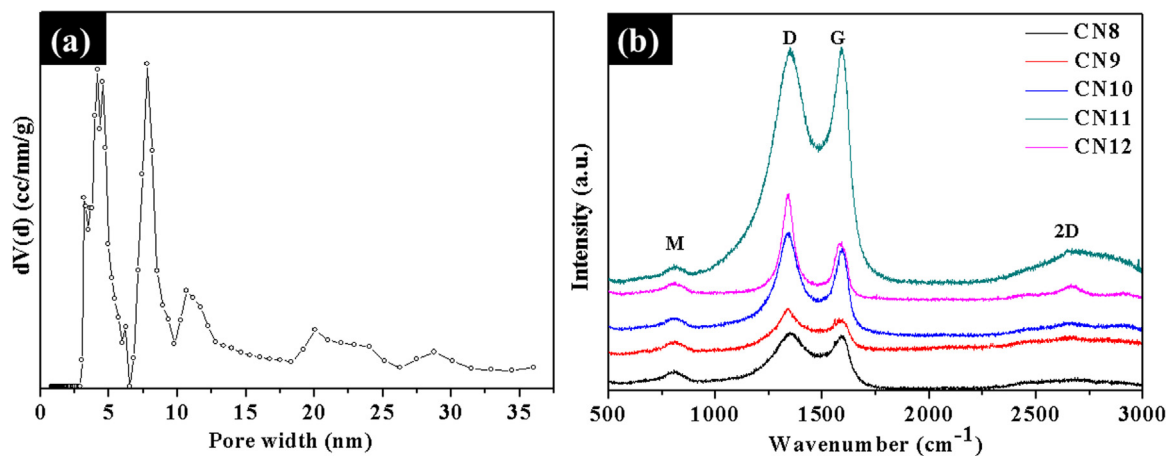

Fig. 2. (a) Pore size distribution of CN10 foam, and (b) Raman spectra of carbon foam samples.
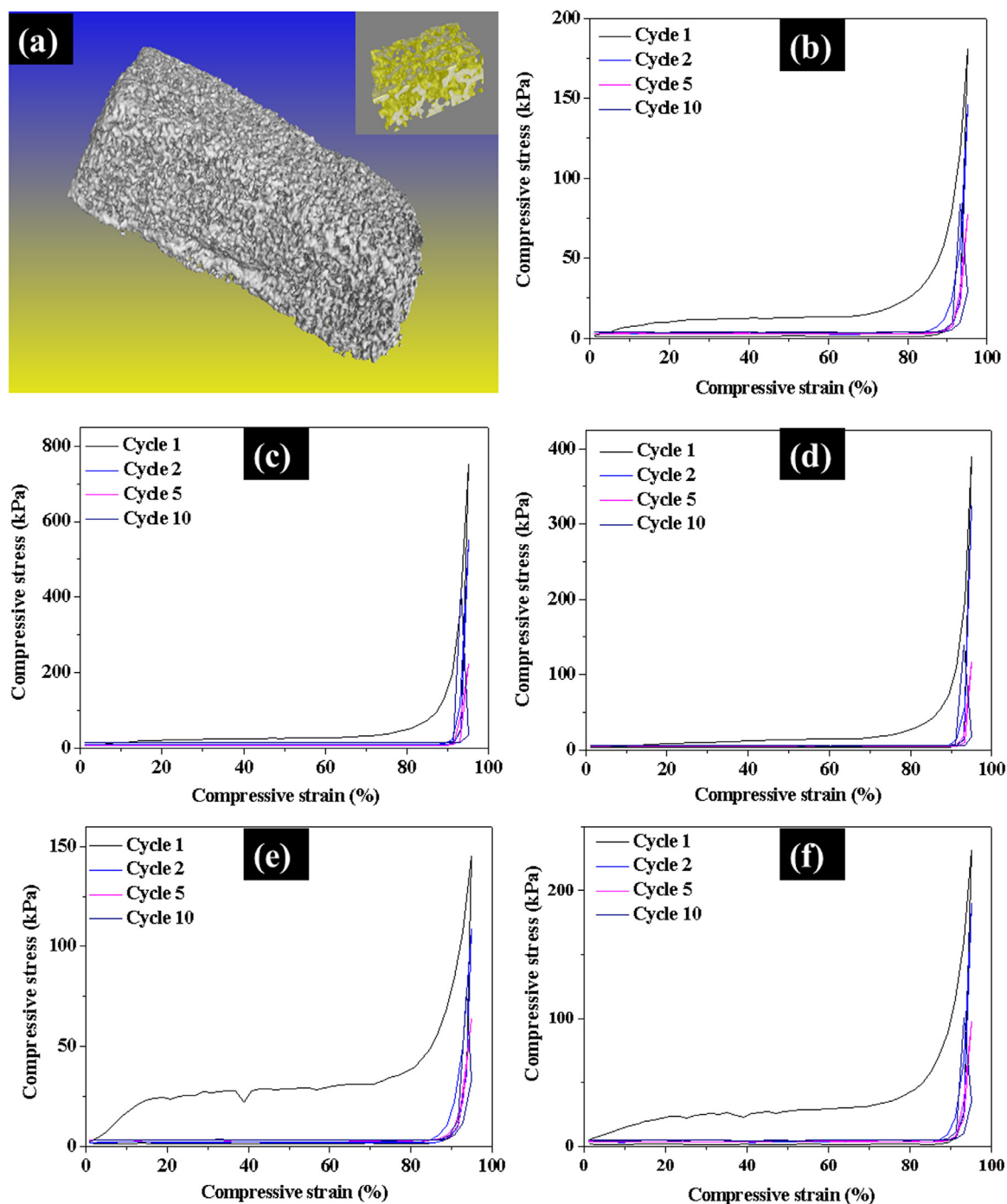
Fig. 3. (a) Micro-CT image of CN12 foam and the cyclic compression stress-strain curves. (b) CN8, (c) CN9, (d) CN10, (e) CN11, and (f) CN12 foams at 95% strain.

(Fig. 1, inset in the middle column). After vacuum infiltration of the carbon foams with PCM mix, SEM images confirm that the PCM mix was absorbed in the open pores of the carbon foam (Fig. 1a-c). No obvious phase separation of the GNP in the PCM mix was observed, and the PCM mix remained inside the pores of the network after absorption (Fig. 1, right column).

Pore size distribution of the carbon foam determined by nitrogen adsorption show a broad range of sub-meso pores within 3–35 nm which were derived from the carbon nanoparticles present on the wall and surface of the foam matrix. These results confirm the presence of mesopores (Fig. 2a). The Raman results of the carbon foams shown in Fig. 2b have confirmed that all samples possess peaks at 1343–1358 cm^{-1} and 1538–1573 cm^{-1} which are assigned to the D and G band of carbon. The D band represents the breathing mode in rings originating from disorder-induced carbon; whilst the G band corresponds to the C-C stretching mode in both chains and rings of graphitic carbon. Peaks present at frequencies within the range of 804.7–810.8 cm^{-1} (marked by M) are linked to the out-of-plane N-C-N bending of melamine [12,13] which originates from porous polymer template. CN11 and CN12 show the 2D peaks at ~ 2680 cm^{-1} which is linked to the overtone of the D band and high energy second order process in graphene. Hence, the foams have a sp^2 carbon network which might contribute to the thermal conductivity.

The strut layout of the 3D network of CN12 foam obtained using micro-CT is shown Fig. 3a. In solid-liquid PCM systems, the mechanical properties of the foam is critical for the form stability and liquid leakage

prevention while maintaining thermal stability and controlling volume changes during phase transitions [6]. Embedding PCM in the foam has several benefits which includes shape stabilization during PCM phase change from solid to liquid, protecting the PCM against the influences of the outside environment while its flexibility can withstand volume changes to improve overall stability. As shown in Fig. 3b–f, the carbon foams are flexible and exhibit excellent mechanical stability at large cyclic strains of up to 95%. The compressive behavior is similar to other open celled foams where an elastic region precedes plateau and densification regions that are triggered by increased stress [14]. The first cycle is different from other cycles because the stress response and hysteresis loop generated during loading and unloading are usually higher. During subsequent cycles, the induced stress response and hysteresis loop gradually decreases till it reaches a constant stress amplitude. Eventually, loading and unloading path reaches a steady state, displaying a shape memory characteristic along a given loading path [15].

After the release of the compressive force, all forms can recover most of deformation elastically, and the 3D interconnected porous structure retains without apparent structural damage, even after 10 cycles. The cyclic compression measurements appear to be nearly

reproducible and all curves return to the original state, with a small plastic deformation of less than 5%. The maximum compressive strength of ~ 800 kPa was obtained for CN9. This excellent cyclic behavior of these carbon foams is highly desirable for coping with and stabilizing the dimensional changes of the PCMs during thermal cycling.

3.2. Shape stabilization of PCM mix and carbon foam nanocomposite

Fig. 4 shows the observations during shape stability of the PCM mix and carbon foam nanocomposites. Between 30 and 58 °C (melting point of PCM), all samples including the PCM mix remain as solid with defined shapes. An increase in temperature above 60 °C, the PCM mix starts to melt and loses its structural integrity. All carbon foam nanocomposites maintain their structural integrity with no obvious leaking of the PCM. At 90 °C, the PCM mix is completely transformed into liquid state, and some PCM mix is observed on the surface of the carbon foam nanocomposites. Varying degree of PCM mix is observed at the bottom of the CN8 and CN9 nanocomposites, and more for CN8.

Apart from CN8 and CN9, all other carbon foam nanocomposites exhibit outstanding shape stabilization up to 100 °C specifically for
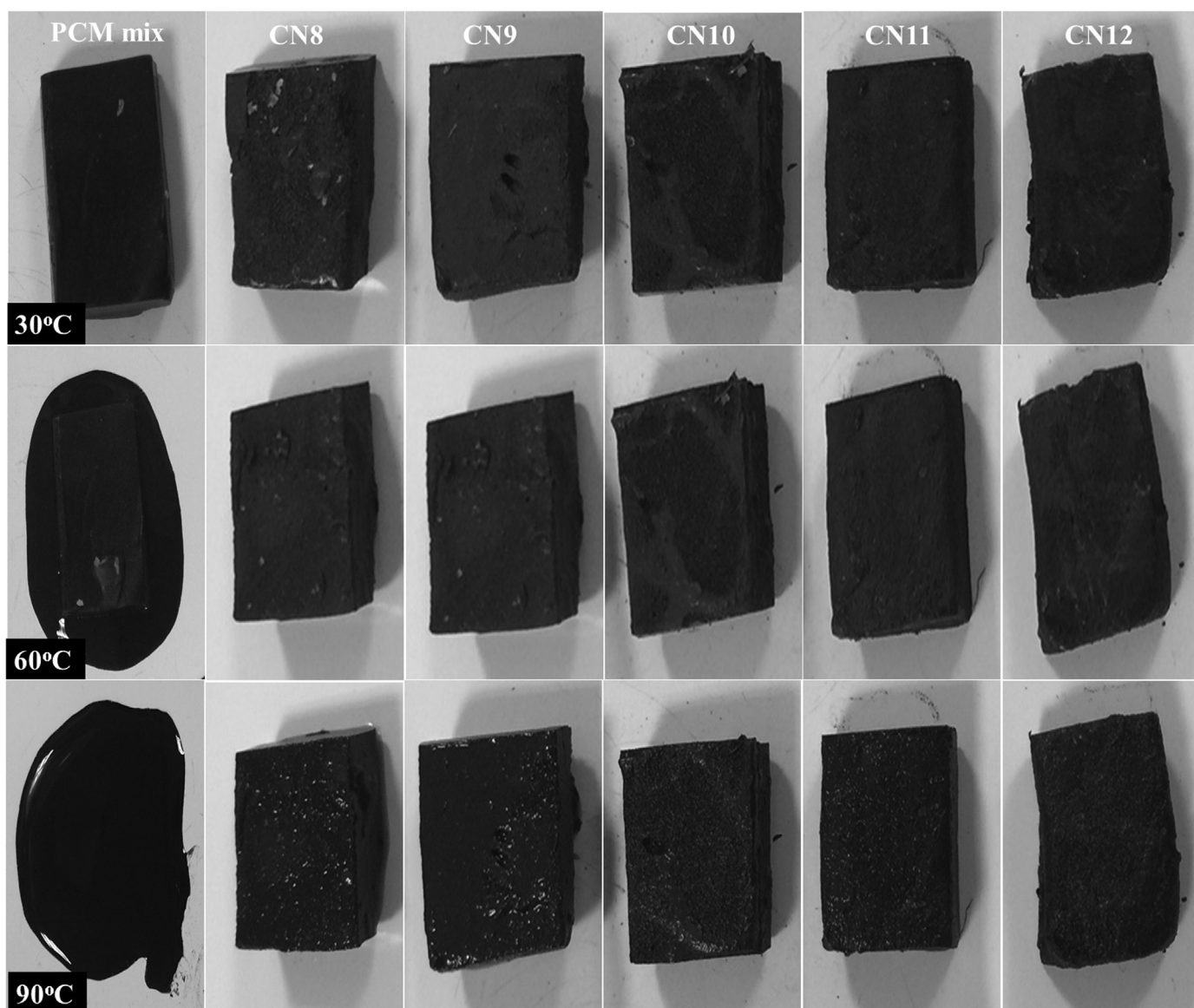

Fig. 4. Observation during shape stability studies of the PCM mix and different carbon foam nanocomposites as a function of temperature.
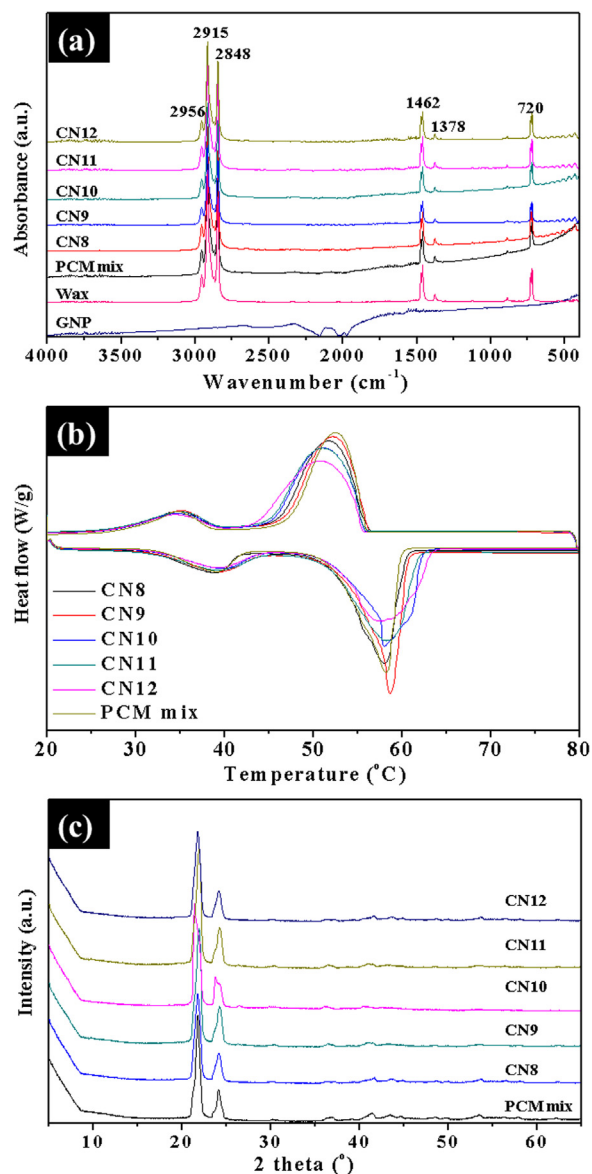
Fig. 5. (a) ATR-FTIR spectra, (b) DSC heating and cooling curves and (c) X-ray diffraction patterns of the PCM mix and various carbon foam nanocomposites.

tested PCM (paraffin wax), since no PCM mix was observed during the entire heating process. The shape stabilization effect of the nanocomposite is mainly linked to the strong physical interaction between the PCM mix and interconnected porous network of the carbon foams. Since the surface of the carbon foams are hydrophobic, they provide better adhesion to the PCM mix such that liquid PCM mix can be readily absorbed into the foam by the pores of the foam acting as capillaries.

PCM mix is also easily absorbed through strong capillary force and surface tension into the open cell foams with high porosity (~ 99% volume weight) and wide pore size distribution range. Overall, this result clearly demonstrates that the flexible, 3D meso-/macroporous network of the carbon foams has facilitated the shape stabilization of the vacuum infiltrated PCM mix, via capillary and surface tension forces holding the liquified PCM mix from escaping from the porous network. Due to the robust mechanical integrity and layered meso-/macroporous morphology of these carbon foams, the nanocomposites are well equipped to cope with volume changes during thermal cycling.

3.3. Phase change behavior of the PCM mix and carbon foam nanocomposites

The interaction between PCM mix and carbon foams were evaluated using ATR-FTIR. Fig. 5a shows the ATR-FTIR spectra of GNP, paraffin wax, PCM mix and carbon foam nanocomposites. PCM mix shows the strong absorbance bands of paraffin wax only due to the low mass concentration of GNP in the PCM mix. Absorption bands at 720 and 1378 cm^{-1} are linked to the in-plane deformation rocking vibration of CH$_2$ group in paraffin wax and the symmetric carbon-hydrogen bending absorption of the CH$_3$ group [16]. The absorption bands at 1462 and 2848 cm^{-1} are primarily assigned to C–H bending vibration and C–H stretching vibration of CH$_2$, respectively. The peak at 2915 cm^{-1} is linked to C–H stretching vibration of CH$_3$. After vacuum infiltration of the PCM mix into the carbon foam, all carbon foam nanocomposites show similar peaks which are referenced to paraffin wax. Clearly, there are no new vibration bands due to no change in molecular structure of paraffin during the hot mixing and ultrasonification of GNP to form the PCM mix. Hence, the nanocomposites retain the chemical stability of paraffin wax.

The capacity, latent heat and phase change temperatures of the PCM mix and nanocomposites were evaluated using DSC. Two phase change peaks are observed in the DSC heating and cooling curves for the PCM mix and nanocomposites, Fig. 5b. The thermal characteristics of the nanocomposites are similar to the PCM mix, as there is no chemical reaction amongst individual components of the nanocomposite. The secondary peaks before ~ 39 °C is assigned to the solid–solid phase transition, while the primary peaks at ~ 58 °C represent the solid–liquid phase transition. The latent heat, estimated by numerical integration of the total area under the peaks, is slightly increased in all nanocomposites except for CN12, compared with the PCM mix. Table 1 lists the onset crystallization/melting temperatures (T_{CO}/T_{MO}), endset crystallization/melting temperatures (T_{CE}/T_{ME}), peak crystallization/melting temperature (T_{CP}/T_{MP}) and enthalpy of crystallization/melting ($\Delta H_{CC}/\Delta H_{MC}$). The enthalpy of crystallization/melting of wax only in the composite PCMs ($\Delta H_{CP}/\Delta H_{MP}$, (J/g)) was normalized using the Eq. (2) where ΔH_C (J/g) and M_g (g) represents the enthalpy of the composite PCMs and the mass fraction of the GNP in the nanocomposite.

$$\Delta HCP/\Delta HMP = \Delta H_C/1 - M_g \qquad (2)$$

The cooling curves of the nanocomposites show slight differences compared with the crystallization behavior of the PCM mix.

Table 1
DSC heating and cooling characteristics of the PCM mix and carbon foam nanocomposites.

Sample	T_{CO} (°C)	T_{CE} (°C)	T_{CP} (°C)	ΔH_{CC} (J/g)	ΔH_{CP} (J/g)	T_{MO} (°C)	T_{ME} (°C)	T_{MP} (°C)	ΔH_{MC} (J/g)	ΔH_{MP} (J/g)
PCM mix	56.00	47.39	52.98	122.52	125.02	53.55	60.81	58.59	123.84	126.37
CN8	55.85	46.22	52.27	126.48	129.06	52.90	59.99	57.66	124.36	126.89
CN9	56.21	46.90	52.75	126.96	129.55	56.34	60.55	57.81	126.72	129.31
CN10	55.71	45.25	52.10	129.84	132.49	51.47	61.58	57.69	127.32	129.92
CN11	55.72	45.52	51.65	125.64	128.20	56.39	62.10	57.65	126.96	129.55
CN12	55.56	43.55	51.20	120.24	122.69	53.15	63.14	57.56	115.92	118.29

T_{CO}/T_{MO}: onset crystallization/melting temperatures, T_{CE}/T_{ME}: endset crystallization/melting temperatures, T_{CP}/T_{MP}: peak crystallization/melting temperature and $\Delta H_{CC}/\Delta H_{MC}$: enthalpy of crystallization/melting, DSC measurement uncertainty: ± 2%.

Nanocomposites undergo a crystallization at lower temperatures due to the GNP interfering with the crystallization. The enthalpy of crystallization of nanocomposites is also influenced by the nucleation, since an increasing trend is observed for samples excluding CN12. The melting temperatures of the nanocomposites also show some slight differences (1.7%) compared with the PCM mix, which might be due to the increased heat transfer from the GNP addition in the PCM mix [17]. The enthalpies of melting slightly increased by 2.8% for all the nanocomposites apart from CN12. In summary, the energy storage density of all nanocomposites apart from CN12 increased compared with the PCM mix. This is due to the conductive network path created by the 3D structure of the carbon foam, which might facilitate an increased phase change speed of the nanocomposites. Another reason for the increased enthalpy might be due to the low mass concentration of GNP compensating the phase change enthalpy rather than replacing the entire PCM [18].

To further evaluate the effect of crystallization on the thermophysical properties of the nanocomposites, XRD was performed. Fig. 5c shows that all nanocomposites possess similar diffraction patterns as the PCM mix. From DSC data, the crystallization temperature was slightly lowered due to the inference of GNP with nucleation. The intensity of the main diffraction peaks at 21.8 and 24.2° which corresponds to (100) and (200) of the paraffin wax became sharper for CN8-CN11, but slightly decreased in CN12. Combined with the DSC and FTIR results, it can be concluded that the PCM mix does not chemically react with the nanocomposites to alter their crystal structure, however a mild effect of promoting its crystallinity has been observed.

3.4. Thermal performance, stability and reliability of the PCM mix and carbon foam nanocomposites

Nanocomposite which consists of the carbon foam, graphene nanoplatelets (2 wt% GNP) and paraffin serves as the structural material, thermal enhancement material and phase change material, respectively. The thermal conductivity of the structural material, carbon foam only is 0.06 W/mK. The thermal conductivity of the PCM mix and carbon foam nanocomposites was measured at different temperatures, from − 50 to 25 °C, and the results are shown in Fig. 6a. Compared with the PCM mix, the thermal conductivities of CN9 - CN11 nanocomposites increased linearly. Sample CN10 exhibits a maximum thermal enhancement of 141% compared to PCM mix. The thermal enhancement demonstrates the contributing role of the carbon foam in creating an effective heat transfer and phonon diffusion through its conductive 3D network. Carbon-based materials have been reported to possess high thermal conductivities [19], and the presence of graphitic carbon in the foam matrix can enhance the thermal performance. Poor thermal enhancement could be linked to the presence of high carbon clusters in

CN12 (Fig. 1c), which restricts the amount of PCM mix absorbed, resulting in a lower latent heat from DSC results. Although CN8 does not possess high carbon clusters, the foam matrix is composed of mainly amorphous carbon. After being filled with the PCM mix, the amorphous structure does not exhibit the maximum thermal enhancement, due to its poorer thermal conductivity.

Thermal stability of PCM mix and carbon foam nanocomposites was evaluated by TGA, and the results are shown in Fig. 6b. Thermal decomposition was not observed for all samples within their phase change temperatures. A comparison of the TGA thermograms of nanocomposites with the PCM mix shows a shift to higher temperature up to 9% for the initial decomposition temperatures of the nanocomposites. These results indicate that the nanocomposites can slow down the thermal degradation while maintaining excellent thermal stability. Thermal decomposition of PCM mix was performed in the programmed temperature range of 220–330 °C through a one-step degradation. Its weight loss at 290 °C can be ascribed to the breakage of paraffin chains during decomposition of volatile organic compounds. The weight loss for the nanocomposite commenced from 300 °C, compared with 290 °C for the PCM mix, implies that the thermal stability was improved by the 3D network of the carbon foam. Thus, the nanocomposites PCM are thermally more stable than the plain paraffin wax which starts to thermally degrade at 150 °C [20].

The transient temperature response behavior and heat transfer capacity of the carbon foam nanocomposites were examined using infrared thermography. Nanocomposites were placed on a hot stage of 100 °C. The temperature response during heating and cooling was recorded with an infrared thermal imager. The temperature distribution images of the nanocomposites recorded at 0, 30 and 70 s during heating are shown in Fig. 7.

Thermal images of the nanocomposites show that the maximum hot zone is at the edge. After 70 s, the samples have rapidly absorbed heat and retained the heat during the heating cycles. As cooling time increases, the samples become greenish-yellow from inside out indicating that the heat is being discharged from the surface during the temperature drop. The chemical and thermal stability of the nanocomposites were further evaluated over several melting and freezing cycles. After 100 thermal cycles, the results of change in chemical structure and thermal properties of sample CN10 are shown in Fig. 8a-b. CN10 shows a negligible change in thermal properties and chemical structure after cycling. DSC curves of CN10 after different cycles of 1, 50 and 100 are shown in Fig. 8a. Negligible changes in the latent heat and phase change temperatures of melting and crystallization were observed.

After thermal cycling up to 100 times, the latent heat of melting and crystallization was almost identical, with a negligible reduction of 0.18% and 0.68% being observed for CN10, respectively. Based on the negligible changes in thermal stability after 100 cycles, it can be
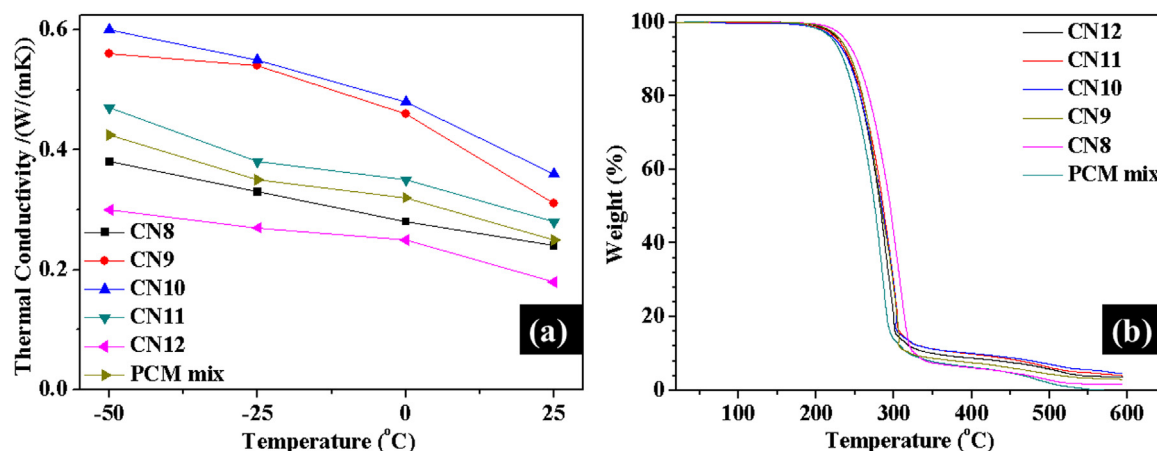

Fig. 6. (a) Thermal conductivity and (b) TGA curves of the PCM mix and different carbon foam nanocomposites.
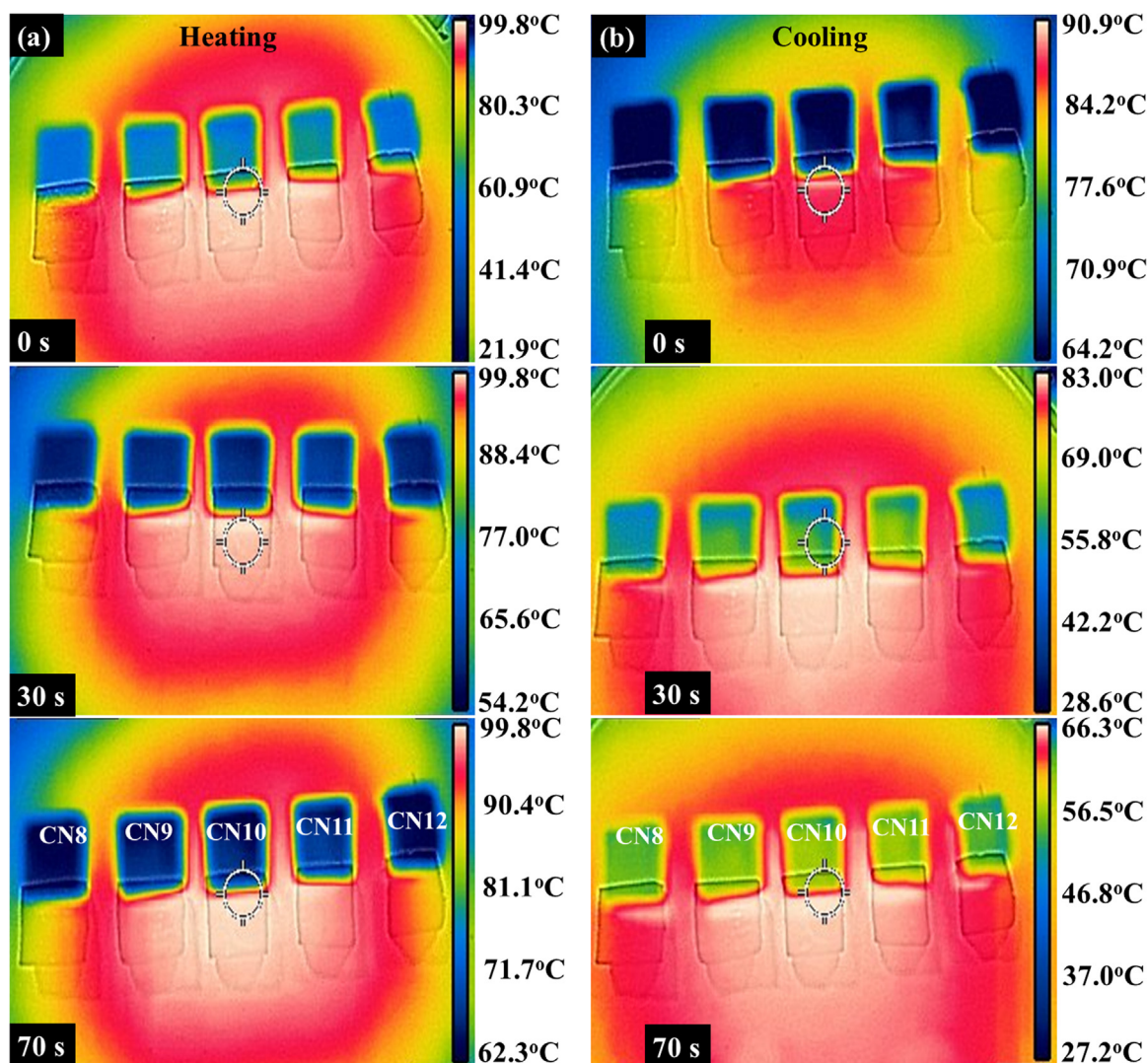
Fig. 7. Temperature distribution images of the carbon foam nanocomposites during heating and cooling for 0, 30 and 70 s (images of CN8–CN12 can be viewed from left to right and the rectangular boxes under the images were caused by shadows).
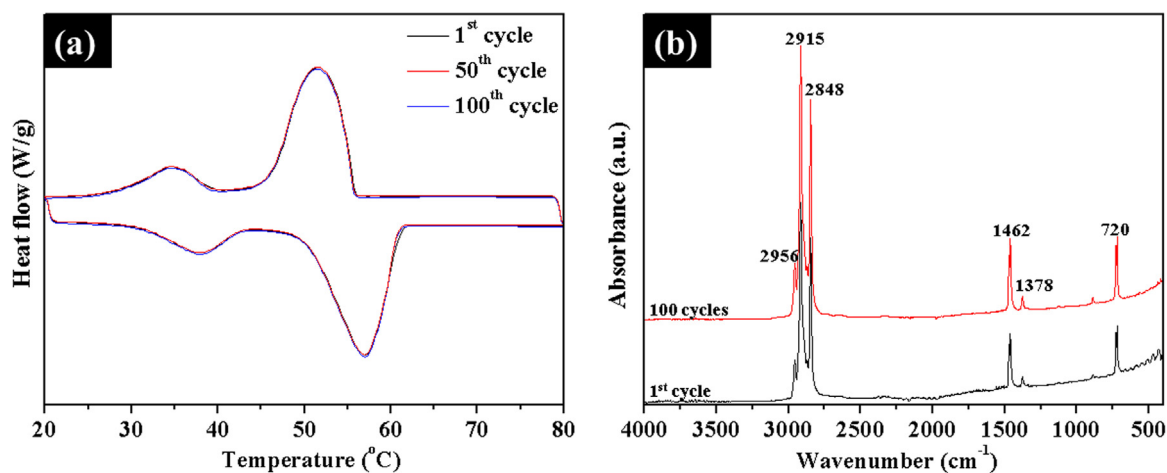

Fig. 8. (a) DSC curves and (b) FTIR spectra of CN10 after 100 thermal cycles.

deduced that CN10 possesses good thermal reliability and is promising for space heating applications. As shown in Fig. 8b, the identical FTIR spectra of CN10 taken before and after 100 cycles further confirm its high thermal stability. The presence and disappearance of new and old vibration peaks was not observed. Thus, it confirms that the chemical structure of CN10 was not modified by thermal cycling. Overall, these findings demonstrate the superior performance of CN10 compared with other nanocomposites, due to its combined properties of excellent shape stabilization, chemical compatibility energy storage density and thermal conductivity.

4. Conclusions

This work demonstrates a new strategy of using 3D carbon foams as the supporting material to accommodate a PCM mix of paraffin wax and GNPs to form nanocomposites for TES applications. The ultralight carbon foams exhibit excellent mechanical properties that is crucial for shape stabilization during dimensional changes from thermal cycling. Investigations into the formulation, chemical compatibility, phase change behavior, thermal stability and reliability of the nanocomposites have shown that the carbon foam is able to retain the PCM mix while enhancing its thermal conductivity. The infiltration of PCM mix into different carbon foams improved the shape stabilization due to capillary effect and surface tension provided by its highly porous and 3D matrix. Apart from maintaining good thermal reliability and stability after 100 thermal cycles, an impressive 141% improvement in the thermal conductivity for sample CN10 has been achieved. This work represents a novel, simple, and cost-effective way to fabricate high-performance materials for TES applications.

Acknowledgments

Competing interests

The authors have no competing interest to declare.

Appendix A. Supporting information

Supplementary data associated with this article can be found in the online version at doi:10.1016/j.solmat.2018.11.037

References

[1] R.K. Sharma, P. Ganesan, V.V. Tyagi, H.S.C. Metselaar, S.C. Sandaran, Developments in organic solid–liquid phase change materials and their applications in thermal energy storage, Energy Convers. Manag. 95 (2015) 193–228.

[2] Z. Zhang, X. Fang, Study on paraffin/expanded graphite composite phase change thermal energy storage material, Energy Convers. Manag. 47 (2006) 303–310.

[3] M. Li, Q. Guo, S. Nutt, Carbon nanotube/paraffin/montmorillonite composite phase change material for thermal energy storage, Sol. Energy 146 (2017) 1–7.

[4] F. Ye, Z. Ge, Y. Ding, J. Yang, Multi-walled carbon nanotubes added to Na2CO3/MgO composites for thermal energy storage, Particuology 15 (2014) 56–60.

[5] Z. Ge, F. Ye, Y. Ding, Composite materials for thermal energy storage: enhancing performance through microstructures, Chemsuschem 7 (2014) 1318–1325.

[6] K. Pielichowska, K. Pielichowski, Phase change materials for thermal energy storage, Prog. Mater. Sci. 65 (2014) 67–123.

[7] Y. Cai, Q. Wei, F. Huang, S. Lin, F. Chen, W. Gao, Thermal stability, latent heat and flame retardant properties of the thermal energy storage phase change materials based on paraffin/high density polyethylene composites, Renew. Energ. 34 (2009) 2117–2123.

[8] S.-G. Jeong, S. Jin Chang, S. We, S. Kim, Energy efficient thermal storage montmorillonite with phase change material containing exfoliated graphite nanoplatelets, Sol. Energy Mater. Sol. Cells 139 (2015) 65–70.

[9] S. Chen, et al., Elastic carbon foam via direct carbonization of polymer foam for flexible electrodes and organic chemical absorption, Energy Environ. Sci. 6 (2013) 2435–2439, https://doi.org/10.1039/C3EE41436A.

[10] X. Gui, et al., Carbon nanotube sponges, Adv. Mater. 22 (2010) 617–621.

[11] Z. Chen, W. Ren, L. Gao, B. Liu, S. Pei, H.-M. Cheng, Three-dimensional flexible and conductive interconnected graphene networks grown by chemical vapour deposition, Nat. Mater. 10 (2011) 424.

[12] L. Stagi, D. Chiriu, A. Ardu, C. Cannas, C.M. Carbonaro, P.C. Ricci, Luminescence enhancement by energy transfer in melamine-Y2O3:Tb3+ nanohybrids, J. Appl. Phys. 118 (2015) 125502.

[13] M. Prabhaharan, A.R. Prabakaran, S. Gunasekaran, S. Srinivasan, Molecular structure and vibrational spectroscopic investigation of melamine using DFT theory calculations, Spectrochim. Acta A 123 (2014) 392–401.

[14] T.N. Pham, et al., Robust hierarchical 3D carbon foam electrode for efficient water electrolysis, Sci. Rep. 7 (2017) 6112.

[15] J. Suhr, et al., Fatigue resistance of aligned carbon nanotube arrays under cyclic compression, Nat. Nanotechnol. 2 (2007) 417.

[16] S.Y. Wu, X. Tong, C.D. Nie, D.Q. Peng, S.G. Gong, Z.Q. Wang, The effects of various carbon nanofillers on the thermal properties of paraffin for energy storage applications, J. Therm. Anal. Calorim. J. Artic. 124 (2016) 181–188.

[17] H. Yang, S.A. Memon, X. Bao, H. Cui, D. Li, Design and preparation of carbon based composite phase change material for energy piles, Materials 10 (2017) 391.

[18] J. Yang, et al., Hybrid graphene aerogels/phase change material composites: thermal conductivity, shape-stabilization and light-to-thermal energy storage, Carbon 100 (2016) 693–702.

[19] A.A. Balandin, Thermal properties of graphene and nanostructured carbon materials, Nat. Mater. Rev. Artic. 10 (2011) 569.

[20] S.A. Memon, W. Liao, S. Yang, H. Cui, S.F.A. Shah, Development of composite PCMs by incorporation of paraffin into various building materials, Materials 8 (2015) 499–518.